# Possibility of coexistence of local-moment and itinerant-electron magnetism in $\alpha$-manganese: A perturbed-angular-correlation study

G. De Doncker, J. Van Cauteren, E. Tieghem, and M. Rots
*Instituut voor Kern, Stralingsfysika, Katholieke Universiteit, Leuven, B-3030 Leuven, Belgium*
(Received 8 January 1988; revised manuscript received 20 December 1988)

Perturbed-angular-correlation techniques using $^{111}$Cd were applied to study the nature of the antiferromagnetism in $\alpha$-Mn. From the hyperfine-field, magnetic dipole, and electric quadrupole interactions, we derived the fact that the indium probe nuclei occupy exclusively site-I positions in the complex crystal structure. The magnetic-ordering temperature was found to be remarkably dependent on the residual impurity level of the material. The magnetic hyperfine field reflects two distinct magnetic sites, with relative population of 70% at the high-field site $B_{hf}=6.33(1)$ T and 30% at the low-field site $B_{hf}=3.10(4)$ T, both measured at $T=4.2$ K. At $T\simeq 20$ K a distinct jump in the hyperfine field is observed at the low-field site only, the magnitude of this jump being somewhat sample dependent. From the observed response of both sites to temperature and applied field, we suggest a coexistence of local-moment and itinerant-electron antiferromagnetism.

## I. INTRODUCTION

Manganese exists in four allotropic forms, two of them stable at room temperature but with rather complex structure. The $\alpha$-Mn phase can be produced by annealing at 600 °C and slow cooling, while the $\beta$-Mn phase results after quenching from high temperature. The basic arrangement of $\alpha$-Mn is body-centered cubic,[1] each lattice point associated with 29 atoms in tetrahedral symmetry. Four inequivalent sites are present with the respective coordination numbers being $C=16$ for site I, $C=16$ for site II, $C=13$ for site III, and $C=12$ for site IV. The interatomic distances vary from 2.26 to 2.93 Å. Neutron diffraction studies[2] have shown that each of the four sites carries a different moment, and that the structure orders antiferromagnetically below $T_N=95$ K. Susceptibility measurements[3] as well as x-ray photoemission spectroscopy[4] of $\alpha$-Mn indicate the existence of large localized moments in the paramagnetic state. A site-dependent model has been proposed[5] in which the large magnetic moments at sites I and II are described by a localized-spin-fluctuation model, while the electronic state for sites III and IV carrying a weak moment can be described by an itinerant-electron-band model. Although the antiferromagnetic ordering in $\alpha$-Mn is not like the itinerant-electron antiferromagnetism of its neighbor chromium, the magnetic ordering may nevertheless be understood as partially due to indirect magnetic coupling mediated by the conduction electrons in which the $d$ electrons play an important role.

In this study we present the first measurement of very-diluted-solute hyperfine-field distributions in $\alpha$-Mn with the aim of verifying whether or not the localized-moment picture fully describes the ordering mechanism. Measurements as a function of temperature as well as external field, we believe, offer enough evidence to suggest that, to a certain extent, a spin-density-wave nature must be added to understand the antiferromagnetism in $\alpha$-Mn.

## II. EXPERIMENTAL DETAILS

### A. Experimental technique

Perturbed-angular-correlation (PAC) spectroscopy was applied on the 173–247 keV $\gamma$-$\gamma$ cascade in the radioactive decay of $^{111}$In to the excited nuclear states in $^{111}$Cd. The intermediate state at 247 keV has a half-life of 84 ns, well suited to observe, time differentially, the nuclear-spin precession induced by the hyperfine interaction between the probe's nuclear moments and extra-nuclear-charge and magnetic-moment distributions. The setup consists of a conventional four-detector arrangement with NaI(Tl) or $BaF_2$ detectors coupled to XP2020(Q) photomultipliers. Data reduction is done by calculating the time-dependent correlation anisotropy $R(t)$ using the expression

$$R(t)=\frac{W_{AC}(\pi,t)W_{BD}(\pi,t)}{W_{AD}(\pi/2,t)W_{BC}(\pi/2,t)}-1\ , \tag{1}$$

where $W_{AC}(\pi,t)$ and $W_{BD}(\pi,t)$ are the true coincidences in a small time interval $\Delta t\leq 2.5$ ns for the detector combination at an angle $\pi$, while $W_{AD}(\pi/2,t)$, and $W_{BC}(\pi/2,t)$ are the corresponding values when the angle between the detectors is $\pi/2$. The perturbed-angular-correlation anisotropy $R(t)$ for the $^{111}$Cd probe sensing a randomly oriented static interaction in a polycrystalline sample can be written in the well-known form as

$$R(t)=A\left[a_0+\sum_{n=1}^{N}a_n\exp(-\delta\omega_n t)\cos(\omega_n t)\right]\ , \tag{2}$$

assuming a Lorentzian distribution $\delta\omega_n$ in the interaction strength measured by $\omega_n$. The coefficient $A$ is determined by known nuclear parameters and the detector geometry. The frequency coefficients $a_n$ depend on texture in the samples and the type of hyperfine interaction. For a static, randomly oriented, magnetic dipole interac-

 

tion we have $a_0=\frac{1}{5}$, $a_1=a_2=\frac{2}{5}$, and $N=2$, while a texturized orientation makes $a_1$ and $a_2$ unequal. For a randomly oriented nonaxially symmetric electric quadrupole interaction ($N=3$) the frequency coefficients depend also on the value of the asymmetry parameter $\eta=(V_{xx}-V_{yy})/V_{zz}$ of the electric field gradient. The interaction frequencies $\omega_n$ (Mrad/s) are given by

$$\omega_n=n\omega_B=n\frac{\mu B}{I\hbar}=n(14.6885B)$$

for a magnetic dipole interaction (where $B$ is in Tesla) and

$$\omega_n=f_n(\eta)\omega_Q=f_n(\eta)eQV_{zz}/\hbar 4I(2I-1)$$

for an electric quadrupole interaction, with $I=\frac{5}{2}$ the nuclear spin, $\mu=-0.7650(25)\mu_N$, $Q=+0.83(2)b$ the nuclear moments in the intermediate state of the $\gamma$-$\gamma$ cascade, $V_{zz}$ is the principal component of the electric field gradient (efg), and $f_n(\eta)$ are the known functions of the asymmetry parameter $\eta$. For axial symmetry, we have $f_1=6$, $f_2=12$, and $f_3=18$ for a nuclear spin $I=\frac{5}{2}$.

Concerning the Mn structure, we expect four[6] or two[1] inequivalent lattice positions available in the $\alpha$- or $\beta$-Mn structures, respectively, and each site is characterized by its particular magnetic hyperfine field and electric field gradient. The latter can be measured separately above the Néel temperature and reflects the charge symmetry at the probe site.

### B. Sample preparation

The starting material was commercially available Mn flakes that were quoted at a purity of 99.99% and etched prior to use with a solution of 5% HCl in methanol. The $^{111}$In activity from a carrier-free $InCl_3$ solution was deposited in an amount typically 20 $\mu$Ci. The material was melted by radio-frequency heating under low argon pressure after evacuation to lower than $10^{-6}$ Torr, resulting in a sample of typically 50–100 mg. The active indium concentration therefore remains in the 0.500 ppb range and may be expected to be homogeneously distributed throughout the sample. Different thermal treatments were subsequently applied, and no loss of indium activity could be noticed, indicating that the radioactive probe is well incorporated in the material.

The thermal treatments of the indium-doped material were different according to the phase required. The sample was annealed at 600 °C for typically 2 h under an argon atmosphere, followed by a slow furnace cooling to produce the $\alpha$-Mn phase. Alternatively, the material was encapsuled in a quartz ampoule evacuated to $3\times10^{-6}$ Torr and filled with low-pressure argon. Annealing at 900 °C for 17 h followed by rapid temperature lowering in liquid nitrogen produced the $\beta$-Mn phase.

As will be illustrated further on, the magnetic-ordering temperature found for $\alpha$-Mn samples prepared from commercially available Mn flakes with Mn powder equals $T_0=120$ K, much above the bulk Néel temperature. For this reason, different conditions for In doping the Mn flakes were investigated: annealing under hydrogen before melting, melting under a mixed argon-hydrogen atmosphere with or without exhaustion in a vacuum, and also ion implantation. In addition, the purity effect was investigated by using material obtained from vacuum distillation[7] of the Mn flakes. In all of the previously mentioned preparation techniques, the hyperfine parameters below the magnetic-ordering temperature were essentially invariant, but the ordering temperature indicated by the Cd probe drops below $T_0=120$ K. At the moment we are not able to explain this unexpectedly large effect which is under further study, although further on we give some preliminary interpretations. Apart from this difficulty, we have enough evidence to argue that the magnetic behavior to be discussed is not affected by the fact that most of the results were obtained on Mn-flake samples.

## III. CHARACTERIZATION OF THE INDIUM ENVIRONMENT

### A. Hyperfine interaction in the $\beta$-Mn phase

In the $\beta$-Mn phase no magnetic ordering is expected[8] at 4.2 K or higher. Therefore, the PAC spectrum should reflect, if anything, an electric quadrupole interaction due to the noncubic symmetry of the lattice. Moreover, two inequivalent lattice positions may be taken by the probe, eventually resulting in two different hyperfine-interaction frequencies. In Fig. 1(a) we display the PAC spectrum measured at $T=77$ K. The data could only be fitted satisfactory with Eq. (2) assuming an electric interaction. Moreover, the data reveal that all probes experience a unique quadrupole interaction with parameters $\omega_Q=26.67(3)$ Mrad/s, $\delta\omega_Q=1.6(2)\%$, and $\eta=0.11(1)$, corresponding with an electric field gradient $V_{zz}=9.15(1)\times10^{21}$ V/m$^2$. These interaction parameters are exactly the same when measured at $T=4.2$ K.

The same sample was subjected to the isochronal-anneal treatment, followed by a measurement at $T=77$ K. Up to annealing temperatures of 500 °C, no significant changes in the interaction parameters were observed, i.e., $\omega_Q=26.5(1)$ Mrad/s, $\delta\omega_Q=2.3(3)\%$, and $\eta=0.13(1)$. After a brief anneal (10 min) at 600 °C, however, the PAC spectrum changes drastically as shown in Fig. 1(b). This spectrum must be analyzed under the assumption of a magnetic interaction at $T=77$ K characterized by the parameters $\omega_B=79.5(1.0)$ Mrad/s and $\delta\omega_B=9.7(2.7)\%$, indicating that we have produced the $\alpha$-Mn phase. Moreover, a sample condition resembling the initial one could be restored in our experiment after a 20-h anneal at 900 °C and quenching. Indeed, the interaction was again quadrupolar with only slight changes in the parameters, i.e., $\omega_Q=25.8(2)$ Mrad/s, $\delta\omega_Q=3.4(7)\%$, and $\eta=0.19(2)$ [see Fig. 1(c)].

The quadrupole interaction we observed here compares fairly well with the quadrupole splitting corresponding to $V_{zz}=3.3\times10^{22}$ V/m$^2$ found at $^{119}$Sn in a Mössbauer experiment[9] on the $Mn_{0.975}Fe_{0.005}Sn_{0.02}$ alloy. The large electric field gradient as well as the asymmetry suggests[10] that the indium atoms occupy site-II positions in $\beta$-Mn. Moreover, this position is taken exclusively because no site characterized by either a zero or small quadrupole in-

teraction could be detected. Although indium impurities are known to induce the largest lattice expansion of all alloys containing nontransition-metal impurities,[11] our sample remained paramagnetic at least down to 4.2 K.

### B. Hyperfine interaction in the $\alpha$-Mn phase

In the paramagnetic state of $\alpha$-Mn we observed at $T=150$ K a relatively small electron-quadrupole interaction with frequency $\omega_Q=1.13(5)$ Mrad/s, corresponding to an axially symmetric electric field gradient $V_{zz}=0.39(2)\times10^{21}$ V/m$^2$. The large distribution width of almost 0.45 Mrad/s shows that the probe environment has, on the average, nearly cubic symmetries and thus is consistent with the tetrahedral symmetry of the type-I position. This site identification is nicely supported by use of purified material from the distillation. Indeed, we observe a large fraction of probes experiencing no perturbation, as reflected by a time-independent anisotropy [see Eq. (1)]. The remaining fraction of the probes, however, senses a similar but weaker quadrupole interaction as measured in the Mn flakes. This is clear proof that all In probe atoms occupy exclusively site-I locations. Each of the other three site possibilities do not have[5] the cubic environment needed to explain the PAC spectrum from the ordering temperature up to room temperature. Interestingly, measurements at higher temperature in the range $T=600-700$ °C indicate the appearance of a new probe site almost 15% populated and characterized by a quadrupole interaction $\omega_Q=11(1)$ Mrad/s. The same site can be quenched in from those temperatures. Most probably, the new frequency is the fingerprint of In atoms activated to jump into site II.

Upon cooling, magnetic ordering sets in and two distinct magnetic sites appear rather abruptly. In Fig. 2 some typical PAC spectra are displayed together with the frequency distribution. The data in the time domain were fitted according to Eq. (2) for magnetic interaction. The frequency distribution, on the other hand, was obtained by using a multifrequency mapping with 100 steps in the range 0–200 Mrad/s. Obviously, the frequency distributions are peaked near 45 and 94 Mrad/s revealing the existence of two distinct sites. The third peak around 180 Mrad/s is an artifact because the PAC spectrum contains $\omega_B$ and $2\omega_B$ as well. The appearance of this peak, however, as well as visual inspection of the PAC spectrum shape, undoubtedly proves the existence of *two* hyperfine fields. Over the whole temperature range down to 4.2 K the interaction frequencies corresponding to the two sites remain in a ratio close to 1:2, while the relative population of the highest interaction site remains at

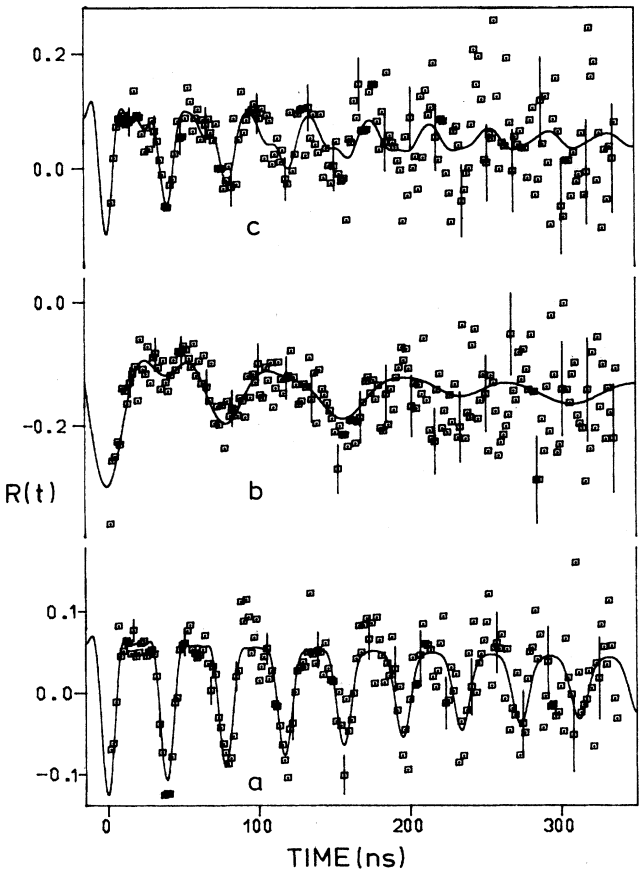


FIG. 1. Spin-precession patterns for $^{111}$Cd in manganese at 77 K illustrating the phase transformation depending upon the heat treatment (a) as quenched from 900 °C: $\beta$-Mn; (b) annealed at 600 °C: $\alpha$-Mn; (c). Reanneal at 900 °C and quench: $\beta$-Mn.

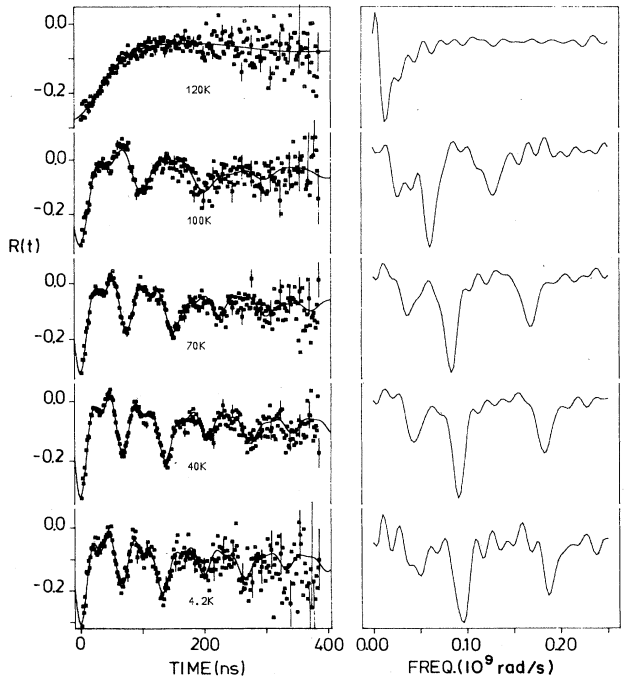


FIG. 2. Time-differential PAC spectra for $^{111}$Cd in $\alpha$-Mn and the derived frequency distributions as a function of temperature. Below the magnetic-ordering temperature $T_N=120$ K the frequency distribution is double peaked indicating two hf-field sites.

63(3)%. All probes contribute to one of the two sites and no paramagnetic fraction could be observed. The respective hyperfine fields at 4.2 K equal 3.24(4) and 6.46(2) T. The hyperfine-field distribution width equals 0.29(5) and 0.22(3) T at the low- and high-field sites, respectively. The width is almost temperature independent for the low-field site but increases beyond $T=90$ K gradually towards 0.48(12) T just below the ordering temperature for the high-field site. The temperature dependence of both hyperfine fields (shown in Fig. 3) reveals that below $T=20$ K a small but significant field increase appears in the low field but clearly not in the high field (see insert). The critical region was not measured here and therefore we have to estimate the exact transition temperature. This was done by a nonlinear least-squares fit of the reduced hyperfine fields $h(T)=H_{hf}(T)/H(4.2\text{ K})$ to an expression of the form[12]

$$h(t)=Bt^{\beta}(1+at^{\Delta}) \quad \text{with } t=1-\frac{T}{T_0} \tag{3}$$

allowing a broad temperature range by including the correction-to-scaling term. Keeping $\Delta=0.50$, the fitted ordering temperature equals $T_0=120.14(5)$ K using all high-field-site data points down to 4.2 K. With the other parameters $B=2.09(2)$, $\beta=0.505(6)$, and $a=-0.522(5)$, Eq. (3) reproduces the hyperfine fields quite well.

### C. Comment on the observed Néel temperature

From resistivity experiments,[13] one knows that substantial shifts in the Néel temperature correlate with the impurity type being, with respect to manganese, either to the left or the right in the periodic table. The former type of impurities apparently replace the large-magnetic-moment atoms on site I or II, the latter impurities substitute the low-moment site III and IV atoms. The Néel temperature in pure $\alpha$-Mn has been determined at $T_N=95$ K with a variety of techniques[1,5,6] including neutron diffraction, resistivity, susceptibility, NMR, and ESR. Most of the present measurements were performed on commercially available Mn flakes of a quoted purity of 99.99%, but during sample preparation Mn powder of >99.9% purity was added to dilute the In concentration. The ordering temperature of those samples repeatedly turned out to be 120 K within almost 2 K. On the contrary, when purified (vacuum-distilled) material was used the ordering temperature substantially reduced and became very much sample dependent. Moreover, we could establish a correlation between the fraction of probes experiencing a weak quadrupole interaction above, say, $T=150$ K and the fraction of the high-field site below the Néel temperature. Even in samples having the expected $T_N=95$ K ordering temperature, the fraction of probes in the high-field site produce a quadrupole interaction of at least $\omega_Q=0.5(1)$ Mrad/s. Very clearly, the low-field site corresponds to In probe atoms in a perfect cubic symmetric environment, as measured above $T_N$ by the proportion of constant anisotropy (the zero quadrupole interaction). In a run on purified material, the temperature dependence of the hyperfine field could be reproduced with the parameters of Eq. (3), now equal to $B=1.70(1)$, $\beta=0.371(3)$, and $a=-0.415(5)$ with $\Delta=0.50$, resulting in a perfect fit to the high-field data. The fitted ordering temperature $T_0=100.2(1)$ K approaches the bulk Néel temperature. The hyperfine-field data of this run are collected in Table I. Also in this sample, the previously observed hyperfine interaction characteristics are essentially reproduced, but we notice an increase in the field ratio between the high-field and low-field sites towards 2.28 and 2.45 below and above $T=25$ K respectively, again revealing the field jump in the low-field site only.

The bulk Néel temperature of 95 K was observed for samples obtained with vacuum-exhausted Mn annealed under vacuum in a tantalum crucible. The temperature behavior of both field sites in the vicinity of the ordering temperature can be described by the exponent $\beta=0.34(1)$. In the present stage of the investigation, most probably, oxygen contamination is responsible for the $T_N$ shift although even the minute In concentration may play an important role. Whatever the reason may be for the important shift in ordering temperature, we con-

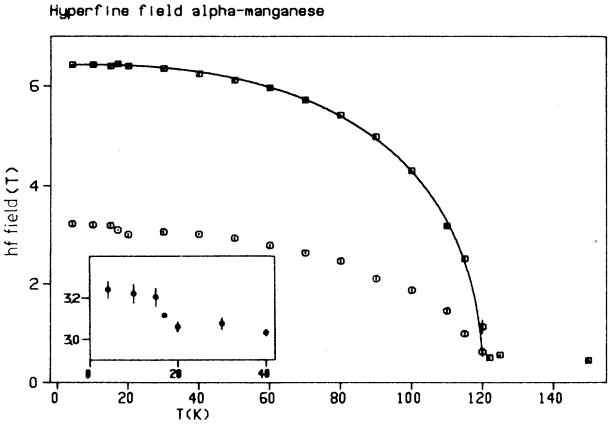


FIG. 3. The temperature dependence of the hyperfine field at the $h$ and $l$ site. Inset: hf-field jump around $T=17$ K in the low-field site.

TABLE I. Magnetic hyperfine fields $B_{hf}$ at $^{111}$Cd in $\alpha$-Mn. $h$: high-field site; $l$: low-field site; $\delta B_{hf}$: full width.

| $T$ (K) | $B^h_{hf}$ (T) | $\delta B^h_{hf}$ (T) | $B^l_{hf}$ (T) | $\delta B^l_{hf}$ (T) |
|---|---|---|---|---|
| 4.2 | 6.75(1) | 0.22(4) | 2.96(7) | 0.38(14) |
| 20 | 6.67(1) | 0.08(2) | 2.91(4) | 0.42(8) |
| 25 | 6.63(1) | 0.06(2) | 2.69(4) | 0.28(10) |
| 30 | 6.58(1) | 0.12(2) | 2.76(4) | 0.30(10) |
| 36 | 6.51(1) | 0.10(2) | 2.74(3) | 0.36(8) |
| 40 | 6.48(1) | 0.14(2) | 2.59(4) | 0.22(10) |
| 50 | 6.34(1) | 0.14(4) | 2.71(10) | 0.24(24) |
| 60 | 6.05(1) | 0.16(4) | 2.44(12) | 0.41(15) |
| 70 | 5.69(1) | 0.18(4) | 2.21(44) | 0.50(10) |
| 95 | 3.48(2) | 0.58(6) | 1.30(1) | 0.88(40) |
| 100 | | | 1.22(7) | 1.42(26) |
| 105 | | | 0.47(7) | 0.70(18) |

clude from the reproducibility in the hf-field data for a variety of sample conditions that the magnetism discussed here concerns elemental $\alpha$-Mn.

### D. Interpretation of the results

The present PAC spectra clearly indicate two distinct magnetic-hyperfine-field distributions in $\alpha$-Mn with mean values in the ratio of 1:2.3. Nevertheless, the crystallographic structure is body-centered cubic with *four* inequivalent sites. So one temperature point $T=40$ K was measured with high statistical accuracy in order to try to unravel the PAC spectrum into four sites. Although the $\chi^2$ values using four frequency components slightly improve over the fit with two frequency components, we reject the former possibility because the frequency components found in the four-site model are already incorporated in a two-component distribution as the one pictured in Fig. 2. Moreover, the fitted relative abundance of the four sites does not even resemble the one expected crystallographically.

Neutron-diffraction studies[1,2] have shown that local moments of $1.9\mu_B$, $1.7\mu_B$, $0.6\mu_B$, and $0.2\mu_B$ exist at the four inequivalent sites I, II, III, and IV, respectively, in $\alpha$-Mn. From atomic packing considerations the relatively large indium atom is better accommodated into the larger volume available at sites I and II compared to the more compact structure at sites III and IV. As in our experiment, we are probing the transferred hyperfine field (Cd is not likely to have a local moment); one estimates a hyperfine-field ratio of almost 1.6:1 at type-I to type-II positions on the basis of a localized-moment model while a ratio of 2.3:1 is found. However, the possibility that the In probe occupies site-II positions is unlikely for two reasons: (i) the abundance of both field sites, and (ii) the quadrupole interaction data. Indeed, below $T_N$ the high-field site is the prominent component in our spectra although the ratio of the crystallographic abundances between site I and site II is 1:4. In addition, the occupancy of the low-field site sensitively depends on the residual impurity level. Identifying the high-field site on the basis of the hf-field value, with type-I positions of the In probe, the low-field site may eventually be associated with type-II probe locations under the condition that In highly prefers type-I positions in the $\alpha$-Mn structure. However, as previously discussed, our quadrupole-interaction data above room temperature reveal a new site most probably representing site-II probe locations. Moreover, NMR results[5] show that the efg at the three noncubic sites are nearly the same and of the order of magnitude of the efg in site-II ($\beta$-Mn).[10] The latter position was measured also in the present work and found to be almost 20 times the value seen in $\alpha$-Mn. Therefore, we are led to the conclusion that indium atoms introduced into $\alpha$-Mn reside almost exclusively on type-I positions. The residual quadrupole interaction observed appears to be correlated with the degree of purity (in the ppm range) of the sample.

One may thus argue that the low-field site corresponds to a probe-impurity complex, in view of the strong impurity effect on the ordering temperature. This interpretation, however, can be denied easily by the observation (above $T_N$) of a distorted cubic environment for a fraction of probes corresponding with the high-field-site population (below $T_N$). Especially this high-field site behaves normally under the influence of an external field, much in contrast with the anomalous behavior at the low-field site, as will be discussed in the next section. Moreover, because the low-field value is nearly half the high-field value, one should expect a rather close probe-impurity configuration, which likely reflects in a much larger quadrupole interaction. Furthermore, the hyperfine field in MnO that we measured with the $^{111}$Cd probe equals $H_{\rm hf}$ (4.2 K)$=18.7(4)$ T, almost an order of magnitude larger than the low-field-site hyperfine field in $\alpha$-Mn. The question that thus arises is why crystallographically identical probe locations are distinct in hyperfine-interaction parameters. As shown in the inset of Fig. 3, we observe a jump of almost 5% in the magnitude of the hyperfine field of the low-field site within a temperature interval of 5 K; this indicates that also the temperature dependence of the hyperfine field at both sites behaves differently. This behavior resembles the temperature-dependent hf-field result obtained[14] with the same technique and the same probe in pure chromium. In that matrix the field increases in a similar way at the spin-flip transition temperature ($T=123$ K) where the magnetization becomes parallel to the spin-density-wave (SDW) vector. The magnitude of the hyperfine field measured at 4.2 K on $^{111}$Cd nuclei in a chromium host equals $H_{\rm hf}=6.2(2)$ T or $\omega_B=90(3)$ Mrad/s and the existence of the SDW is well documented.

We are not aware of conclusive experiments supporting or rejecting the spin-density-wave picture for $\alpha$-Mn. Furthermore, no information is available on any transition at low temperature. Whether or not the low-field site in our data can be explained as revealing an Overhauser distribution in the hyperfine-field magnitude may, in principle, be derived from the PAC spectrum shape. As discussed in more detail in the chromium work[14] for such a distribution, the PAC spectrum contains a sum of zero-order Bessel functions instead of simple cosine functions, the latter corresponding to a $\delta$-function-type hyperfine-field distribution. Detailed analysis of our data could not give any indication that such an interpretation model is preferable for the low-field site. The fact that the two frequencies are in a ratio close to 2:1 for the entire temperature region severely limits the sensitivity on the actual shape of the distribution. At low temperature, significantly better data fitting is achieved for a hyperfine-field distribution essentially of the $\delta$-function type, even allowing for a texturized spatial orientation. Near to the Néel temperature we noticed some improvement when the low-field site was given an Overhauser distribution, but then with a very pronounced texture effect. The data fitting using $\delta$-function field distributions for both sites does not involve texture effects. Therefore, we have to conclude that the spin-density-wave vectors, if present, may be commensurate with the dimensions of the unit cell.

To obtain more evidence on the possible coexistence of local-moment magnetism and itinerant-electron magne-

tism in $\alpha$-Mn, we proceed in the next section with experiments under an external polarizing field.

## IV. HYPERFINE INTERACTION UNDER AN EXTERNAL FIELD

In the $\alpha$-Mn phase the dependence of the hyperfine-interaction parameters on an externally applied magnetic field has been investigated under the experimental conditions previously mentioned. The applied-field geometry was perpendicular to the detector plane and appropriate magnetic shielding prevented any field influence on the detectors.

In the first run the effect of the magnetic history of the sample was investigated. For this purpose the zero-external-field measurement at $T=77$ K was performed three times: first, after cooling without a field (ZFC); second, after cooling through the Néel temperature with a 4-T field (FC), and third, after subsequent heating of the sample (without a field) to 200 K followed by zero-field cooling to 77 K. While the hyperfine-field values measured for both field sites remain almost unchanged, the hyperfine-field distribution for the low-field site sharpens drastically from 18% in the ZFC condition to 4.6% in the FC condition. In the high-field site, however, the probe experiences a narrow interaction distribution of 1.7% for all of the three sample conditions investigated. A similar influence of the external field on the low-field-site hyperfine-field distribution was noticed at 4.2 K, although it was not measured in detail. Additional PAC experiments were performed either at constant temperature (4.2 and 77 K, respectively) as a function of the external field or at a fixed polarizing field as a function of temperature.

The hyperfine-interaction parameters derived from the constant-temperature run are collected in Table II and displayed in Fig. 4. In this figure we plot the external field dependence of the hyperfine-field magnitude for 4.2 and 77 K at both field sites in the ZFC condition.

In a polycrystalline sample the observed total field

$$\mathbf{B}_T=\mathbf{B}_{\rm hf}+\mathbf{B}_{\rm ext} \tag{4}$$

should be the result of an averaging over all relative directions between the hf field $B_{\rm hf}$ and the applied field $B_{\rm ext}$. In the low-external-field region and with $B_{\rm ext}\leq B_{\rm hf}$, one expects the observed field $\langle B_T\rangle$ and its distribution width $\Delta B_T=\langle B_T^2\rangle-\langle B_T\rangle^2$ to depend on the applied field according to

$$\langle B_T\rangle=B_{\rm hf}+\frac{1}{3}\frac{B_{\rm ext}^2}{B_{\rm hf}} \tag{5}$$

$$\Delta B_T=\left[\frac{1}{3}B_{\rm ext}^2-\frac{B_{\rm ext}^4}{9B_{\rm hf}^2}\right]^{1/2}\simeq\frac{1}{\sqrt{3}}B_{\rm ext}\ . \tag{6}$$

Except that eventually the data at 4.2 K in the low-field site below $B_{\rm ext}=2$ T, our data actually do not follow such behavior. At least in a field above 0.1 T, the sample does not show spatial randomness in the hyperfine-field orientation. Indeed, the average angle $\langle\theta\rangle$ between $B_{\rm hf}$ and $B_{\rm ext}$ (Fig. 5) as derived from the observed field using the vector sum in Eq. (4) equals 70(1)° and 116(2)° at 4.2 K in the $h$ and $l$ site, respectively, with $B_{\rm ext}=0.1$ T, while $\langle\theta\rangle=90°$ is expected for a random orientation. Applying an increasing field on an antiferromagnet leads us to expect at some field value of $B_{\rm SF}$ a spin-flop transition in which the magnetic spins orient perpendicular to the applied field. Domains with the anisotropy axis close to $\mathbf{B}_{\rm ext}$ will flop at $B_{\rm ext}\geq B_{\rm SF}$, while for domains with the anisotropy axis already perpendicular, no flopping occurs. The overall result is that the magnetic spins tend to lie preferentially in a plane perpendicular to the applied-field direction when the latter is steadily increasing. Because of the polycrystalline nature of our sample, a gradual evolution towards the spin-flop state may be expected. If the hyperfine field we observe originates from the neighboring local Mn moments, the observed total field should follow the evolution of the spins. This is exactly what is observed at the high-field-site probe locations as illustrated in Fig. 4 which shows the field versus the applied field. However, a site-dependent response is clearly illustrated in this figure based on the data of Table II. Comparing the behavior in the low-field site with the one in the

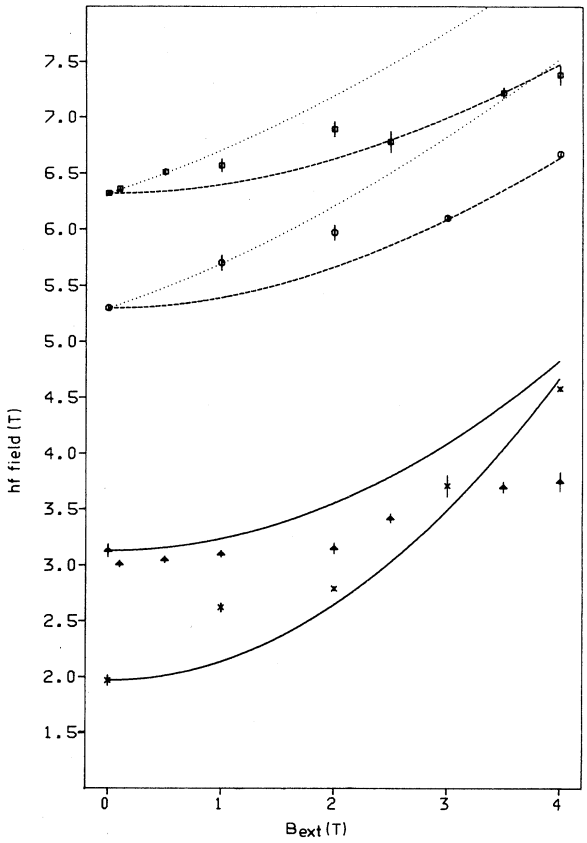


FIG. 4. Total observed field vs external field for high-field and low-field site at $T=4.2$ K (ZFC) and 77 K (FC). ○: high-field site for 4.2 and 77 K, respectively; ▲: low-field site for 4.2 and 77 K, respectively. Pseudorandom geometry [Eq. (7)] with $a=1/3$ and $b=2/3$ and positive signs (dotted curve); with $a=0$ and $b=1$ (dashed curve). Solid line: random geometry [Eq. (5)].

high-field site, a substantial difference emerges.

In the high-field site the observed field increases are comparable at both temperatures, indicating a gradual evolution towards the spin-flop state, where $\mathbf{B}_{hf}$ is perpendicular to $\mathbf{B}_{ext}$ or $B_T=(B_{hf}^2+B_{ext}^2)^{1/2}$ (dashed curve); this state is realized for applied fields above $B_{ext}\simeq 2.5$ T. Assuming that $B_T$ is determined by the relative amount of parallel and perpendicular domains, one estimates the applied field dependence of $B_T$ below $B_{SF}$ as given by

$$\langle B_T\rangle = a(B_{hf}\pm B_{ext})+b(B_{hf}^2+B_{ext}^2)^{1/2}\ , \qquad (7)$$

with $a=\frac{1}{3}$ and $b=\frac{2}{3}$ gradually changing towards $a=0$ and $b=1$ close to and above $B_{SF}$. Below $B_{ext}\simeq 2$ T, the observed field values (high-field site) follow this dependence almost exactly (dotted curve), but interestingly, only the positive sign contributes to the parallel term. Clearly, only the upper hemisphere of a spatially random hf field $B_{hf}$ distribution exists when applying a field. Referring again to Fig. 4, the behavior in the low-field site is completely different in respect to both temperatures 4.2 and 77 K. For the higher temperature a similar gradual evolution towards a spin-flop state may be noticed, although above $B_{ext}=2$ T the field increase is somewhat faster than expected under the previous assumption. At 4.2 K, however, the field increase is much too slow to be understood in that way. Apparently, the gradual rotation of the domains does not occur before $B_{ext}=2$ T. Thus, below this value the external-field effect is negative. This observation reminds one of the hf-field jump occurring below 20 K in the temperature dependence of the zero field hf field at the low-field site (Fig. 3).

One notices from Fig. 4 that the value of the total field, observed with $B_{ext}=4$ T, is higher at $T=77$ K than at 4.2 K. The samples used in those runs, however, differ in magnetic history such that the $T=77$ K data were obtained after field cooling (FC), while the 4.2 K data are for a zero-field-cooled (ZFC) sample. To explore this effect further, we measured the temperature dependence of the observed field in the FC and ZFC sample conditions. Figure 6 shows the time spectra at different temperatures for the FC sample obtained by cooling it from room temperature down to the measuring temperature with $B_{ext}=4$ T on. The corresponding total field $B_T$ values for the low- and high-field sites are plotted in Fig. 7. Clearly, down to 150 K we observe the external field only, while around 120 K the Néel temperature of this particular sample is reached and the hyperfine field develops, again resulting in two distinct sites. Assuming the same temperature dependence of $B_{hf}$ as shown in Fig. 3, the use of Eq. (4) allows us to determine the angle $\theta$ between $\mathbf{B}_{ext}$ and $\mathbf{B}_{hf}$. For the high- ($h$) and low- ($l$) field site, respectively, this angle is $\theta_h=90(2)°$ and $\theta_l=77(3)°$ independent of temperature. The high-field site $B_{hf}$ has an orientation perpendicular to $B_{ext}$, whereas the low-field site $B_{hf}$ has a tendency to align with the external field. It is also clear from Fig. 7 that $B_T$ (4.2 K) is certainly larger than $B_T$ (77 K) in a field-cooled condition.

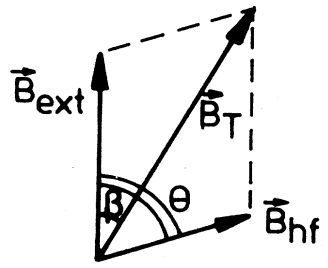


FIG. 5. Geometry between the external field $\mathbf{B}_{ext}$, the hyperfine field $\mathbf{B}_{hf}$ and the observed field $\mathbf{B}_T$ defining the angles $\beta$ and $\theta$.

The ZFC samples were cooled from $T=215$ K (well above $T_N$) to 4.2 K, then $B_{ext}=4$ T was applied and the temperature raised to the measuring temperature. The results are shown in Fig. 8 for both field sites and different temperatures. Using a similar analysis as above the determined values for $\theta_h$ and $\theta_l$ are plotted in Fig. 8. In order to check this derivation, an independent method to determine the $\theta$ values was applied. Indeed, in Eq. (2) the amplitude parameters $a_n$ depend on the orientation of $\mathbf{B}_T$ with respect to the detector plane, and therefore de-

TABLE II. Observed magnetic fields at $^{111}$Cd in $\alpha$-Mn under different external fields. All values in Tesla.

| | $T=4.2$ K | | | | $T=77$ K | | | |
|---|---|---|---|---|---|---|---|---|
| $B_{ext}$ | Low-field site | | High-field site | | Low-field site | | High-field site | |
| (T) | $B_T^l$ | $\Delta B_T$ | $B_T^h$ | $\Delta B_T$ | $B_T^l$ | $\Delta B_T$ | $B_T^h$ | $\Delta B_T$ |
| 0 (ZFC) | 3.13(6) | 0.15(8) | 6.32(1) | 0.18(2) | 2.09(4) | 0.37(4) | 5.19(1) | 0.09(1) |
| 0 (FC) | | | | | 1.97(5) | 0.09(6) | 5.30(1) | 0.07(1) |
| | | | (ZFC) | | | | (FC) | |
| 0.1 | 3.01(3) | 0.00(5) | 6.36(1) | 0.17(2) | | | | |
| 0.5 | 3.05(3) | 0.05(3) | 6.51(3) | 0.28(4) | | | | |
| 1.0 | 3.10(3) | 0.14(4) | 6.57(6) | 0.65(8) | 2.62(4) | 0.05(5) | 5.70(7) | 0.40(9) |
| 2.0 | 3.15(5) | 0.28(6) | 6.89(7) | 0.36(11) | 2.79(2) | 0.17(3) | 5.97(7) | 0.50(9) |
| 2.5 | 3.42(4) | 0.24(6) | 6.78(10) | 0.42(15) | | | | |
| 3.0 | | | | | 3.71(10) | 0.20(15) | 6.10(3) | 0.25(4) |
| 3.5 | 3.70(5) | 0.31(8) | 7.22(5) | 0.37(8) | | | | |
| 4.0 | | | | | 4.58(2) | 0.27(4) | 6.67(1) | 0.12(1) |

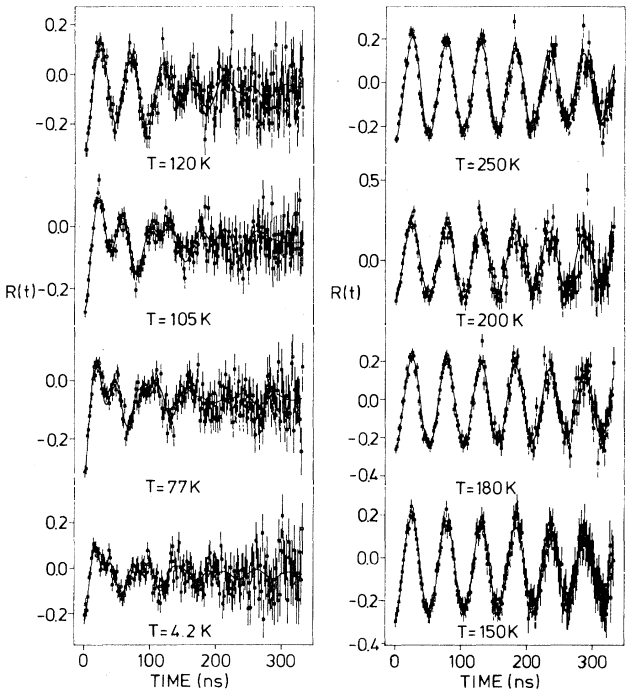


FIG. 6. Spin-precession spectra taken during field cooling in $B_{ext}=4$ T. Above $T_N=120$ K only the influence of the external field is observed.

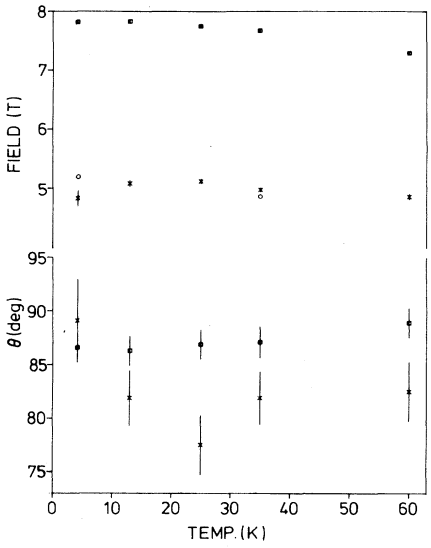


FIG. 8. Total observed field temperature dependence at both sites in the ZFC condition, measured with $B_{ext}=4$ T. For the low-field site, also the FC measurements on the same sample at 35 and 4.2 K are indicated. No jump in the field occurs between these two measurements. Variation with temperature of the angle $\theta$ between $B_{hf}$ and $B_{ext}$ is derived from the total field observed and using Eq. (4).

pend on the angle $\beta$ between $\mathbf{B}_T$ and $\mathbf{B}_{ext}$ (Fig. 5). A set of $a_n(\beta)$ were calculated for $\mathbf{B}_T$ lying on a cone with an angle $\beta$ around $\mathbf{B}_{ext}$, and compared with the amplitudes fitted in the PAC spectrum. This procedure results in essentially the same values of $\theta_h$ and $\theta_l$ as obtained from Eq. (4). We conclude that $\theta_h=87(2)°$ independent of temperature. The low-field site angle $\theta_l$, however, clearly depends on temperature, being almost 90° at 4.2 K the value decreases to a minimum value of 78(3)° at 25 K and levels off at 81(3)° for $T\geq 25$ K. Moreover from Fig. 8 one sees that $B_T$ (4.2 K)=4.83(3) T equals $B_T$ (60 K)=4.86(6) T. A measurement on the same sample, but FC, resulted in $B_T$ (4.2 K)=5.17(7) T, and the downwards jump at $T=17$ K disappears. Thus, whereas the high-field site in the ZFC condition again has the normal temperature behavior, the low-field site shows a distinct jump around 17 K, comparable with the jump around 20 K in the zero-external-field data of Fig. 3. The magnitude of this field jump in $B_T$ turns out to be sensitive to the method of sample preparation, but its occurrence can be explained by a variation of the angle $\theta_l$ between $\mathbf{B}_{ext}$ and $\mathbf{B}_{hf}^{l}$ with temperature. This reorientation of $\mathbf{B}_{hf}$ however does not appear in an FC sample.

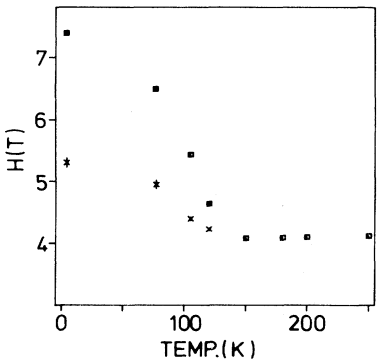


FIG. 7. The observed hyperfine fields as a function of temperature for the FC experiment with $B_{ext}=4$ T.

## V. CONCLUSION

The experiments reported here are the first measurements on hyperfine interaction at very dilute probe nuclei in both $\alpha$-Mn and $\beta$-Mn. In the $\alpha$-Mn phase, we conclude that the indium impurity occupies exclusively site-I positions where the Cd probe experiences a weak electric-quadrupole interaction due to the remaining impurities. In the $\beta$-Mn phase, on the other hand, a well defined, rather large quadrupole interaction was observed with a small asymmetry parameter. Both crystallographic phases could be produced simply depending on whether the sample was slowly cooled or quenched.

No magnetic ordering at 4.2 K was observed in $\beta$-Mn consistent with earlier results. The microscopically determined magnetic-ordering temperature in $\alpha$-Mn is extremely sensitive to the residual impurity level of the material. Furthermore, although the indium probe occu-

pies a single crystallographic position, we observe two magnetically distinct sites. The hyperfine fields at those sites have a different temperature behavior and a different response to an external field. While the high-field site can be well understood by a local-moment picture, the nature of the low-field site should be different. A number of observations specific to the low-field site indicate the possible existence of an itinerant antiferromagnetism reminescent of that in chromium. Field cooling substantially sharpens the hf-field distribution. A jump around $T=20$ K in the hf-field temperature dependence is observed similar to the jump in chromium. The response to an applied field changes as it goes from 4.2 to 77 K. While the high-field site behaves identical in the ZFC and FC conditions, the low-field site shows a decrease of total observed field below 20 K in ZFC samples but not in FC samples. Moreover, the occurrence of the low-field site depends heavily on the sample preparation and the impurity concentration. Whether or not a spin-density-wave picture explains this anomalous behavior of the low-field site remains an open question. Further measurements using single crystals may be conclusive in this respect.

## ACKNOWLEDGMENTS

The authors are indebted to Professor A. Z. Hrynkiewicz (Jagollonian University, Cracow) for stimulating discussions. The help of Dr. O. Arkens (Departement Metaalkunde en Toegepaste Materiaalkunde, Leuven) and W. Schollaert in sample preparation is gratefully acknowledged. This work was financially supported by the Belgian "Interuniversitair Instituut voor Kernwetenschappen."

[1]J. S. Kasper and B. W. Roberts, Phys. Rev. **101**, 537 (1956).
[2]T. Yamada, N. Kunitomi, Y. Nakai, D. E. Cox, and G. Shizane, J. Phys. Soc. Jpn. **28**, 615 (1970).
[3]H. Nagasawa and M. Uchinami, Phys. Lett. **A42**, 463 (1973).
[4]F. R. McFeely, S. P. Kowalczyk, L. Ley, and D. A. Shirley, Solid State Commun. **15**, 1054 (1974).
[5]S. Murayama and H. Nagasawa, J. Phys. Soc. Jpn. **50**, 810 (1981); **50**, 1523 (1981).
[6]H. Nasagawa and M. Senba, J. Phys. Soc. Jpn. **39**, 70 (1975).
[7]T. Yamada, J. Phys. Soc. Jpn. **28**, 1499 (1970).
[8]Y. Masuda, K. Asayama, S. Kobayashi, and S. Itoh, J. Phys. Soc. Jpn. **19**, 460 (1964).
[9]Y. Nishihara, S. Ogawa, and S. Waki, J. Phys. Soc. Jpn. **42**, 845 (1977).
[10]L. E. Drain, Proc. Phys. Soc. **88**, 111 (1966).
[11]T. Kohara and K. Asayama, J. Phys. Soc. Jpn. **37**, 401 (1974).
[12]M. A. Kobeissi, Phys. Rev. B **24**, 2380 (1981).
[13]W. Williams and J. L. Stanford, Phys. Rev. B **7**, 3244 (1973).
[14]R. Venegas, P. Peretto, G. N. Rao, and L. Trabut, Phys. Rev. B **21**, 3851 (1980), and references therein.